



Microstructures, electrical behavior and energy storage properties of Ag@shell/PVDF-based polymers: different effects between an organic polydopamine shell and inorganic zinc oxide shell

Lizhu Guan¹, Ling Weng^{1,2,*} , Xiaorui Zhang^{1,2}, Zijian Wu¹, Qiong Li³, and Lizhu Liu^{1,2,*}

¹ College of Material Science and Engineering, Harbin University of Science and Technology, No. 4 Linyuan Road, Xiangfang District, Harbin 150040, Heilongjiang, People's Republic of China

² Key Laboratory of Engineering Dielectric and Its Application, Ministry of Education, Harbin University of Science and Technology, Harbin 150080, People's Republic of China

³ Department of Molecular Science and Engineering, Case Western Reserve University, Cleveland 44106, USA

Received: 2 May 2020

Accepted: 18 July 2020

Published online:

31 July 2020

© Springer Science+Business Media, LLC, part of Springer Nature 2020

ABSTRACT

Two kinds of 1D core–shell nanorods silver@polydopamine (Ag@PDA) and silver@zinc oxide (Ag@ZnO) were successfully synthesized and doped into polyvinylidene fluoride (PVDF) to fabricate composites. The different surface modification effects between the organic PDA shell and inorganic ZnO shell on structure and dielectric properties of PVDF composites were investigated. Results indicated that the ZnO shell showed a crystalline structure, while the PDA shell is amorphous. Due to the difference in crystal structure of the coating shell, the Ag@ZnO/PVDF composites showed a better dielectric performance than the Ag@PDA/PVDF composites, while the Ag@PDA/PVDF showed excellent mechanical properties. The crystallized structure of ZnO not only promoted the crystal conversion of PVDF molecules, but also effectively limited the movement of charge carriers in composites. In the case of 10wt% fillers' content and before breakdown strength, the energy storage densities of Ag@PDA/PVDF and Ag@ZnO/PVDF composites are 79.53% and 209.2% higher than that of pure PVDF films, respectively. Moreover, the charge/discharge efficiency of Ag@ZnO/PVDF composite is also higher than that of pure PVDF and Ag@PDA/PVDF composite. When testing at 1800 kV/cm electrical strength, the energy storage density of Ag@ZnO/PVDF composite increases to 4.02 J/cm³.

Address correspondence to E-mail: wengling79@163.com; mrliluzhu@163.com

Introduction

Nowadays with the rapid development of electronic products toward miniaturization, as well as intelligent and wearable devices, a lot of higher requirements are being drawn to the electronic components. Dielectric polymer-based composites have attracted much attention in recent years due to excellent flexibility and plasticity, as well as rapid charge/discharge efficiency, stable chemical properties and high energy storage density [1–3]. The key to the performance of dielectric polymer-based composites is the energy storage density, which can be calculated by the formula $U = \frac{1}{2} \epsilon_r \epsilon_0 E^2$ (linear dielectrics) and $U =$

$\int_0^{D_m} EdD$ (nonlinear dielectrics). It is closely related to the parameter of breakdown strength, dielectric loss and dielectric constant [4,5]. One efficient approach to fabricate the composites is to introduce a high dielectric filler into a piezoelectric polymer, but it is hard to adjust all the parameters of the composite to optimal values [6]. Therefore, how to ensure the composites stays at a low loss, and then exhibit a good breakdown strength and large dielectric constant is a really big challenge.

PVDF (polyvinylidene fluoride) is a common dielectric substrate material with an electrical dipole moment of monomer unit ($5\text{--}8 \times 10^{-30}$ cm) which varies with the crystal phase of PVDF [7]. Generally speaking, the β and γ phase usually exhibits superior polarities as it has a more regular polar orientation alignment relative to the α phases, which makes PVDF a good candidate for dielectric materials [8]. The polarity phase of PVDF can be obtained by some processing methods, such as adding some polar fillers (TiO_2 , BaTiO_3) [9,10], copolymerizing with polar groups (poly(methyl methacrylate) (PMMA)) [11], aromatic polythiourea (ArPTU) [12], stretching the molten state of PVDF, polarization at high voltage, etc. It is worth noting, for the approach of adding fillers, that, in addition to the polarization phase transition of the matrix, composites can be specifically modified by different functional fillers through the physical and chemical combination between the filler and the matrix. For example, Zhang et al. [13] and Wang et al. group [14] reported an application of boron nitride nanosheet (BNNS)-modified PVDF in performance energy storage and heat conduction.

Bhattacharya et al. [15] reported a high energy storage PVDF flexible device, through the combination of graphene and red-mud nanoparticles, which is an environmentally friendly material with high energy storage.

Moreover, some researchers also reported that the dielectric anisotropy between fillers and polymers could affect the polarization behavior of polymer-based composites, then further affect its' energy storage performance [16,17]. This dielectric anisotropy highly depends on the structure and morphology of inorganic filler phases. Compared to spherical particles, doping a small amount of 1D or 2D fillers can effectively optimize the macroscopic properties of the composites medium [18–21]. For example, the dielectric constant of a composite doped with BaTiO_3 nanowires is three times higher than that of the composite doped with the same amount of BaTiO_3 particles [22]. However, the introduction of large amounts of inorganic nanoparticles usually leads to a serious agglomeration of fillers and the easy formation of internal conductive paths, resulting in a greater increase in dielectric loss of composites [23]. Growing a shell on the desired conductive nanoparticle is a common practice in nanotechnology to enhance the compatibility between matrix and filler, isolate the agglomeration of central particles and suppress dielectric loss under electric field. For example, Pan et al. [24], modified BaTiO_3 by Al_2O_3 to synthesize new one-dimensional core-shell nanofibers and then dropped them into a PVDF matrix. Results showed that the composites with 5 vol% core-shell nanofibers exhibited an excellent energy density of 12.18 J/cm^3 at 400 MV/m. Huang et al. [25] reported a good review on the impact of core-shell structure on energy storage performance. Furthermore, the results of previous research in our group indicate that the insulating shell Al_2O_3 promotes the polarization of the matrix [26].

Many scholars use inorganic insulators such as SiO_2 to modify particle surfaces to help suppress leakage current [27]. However, relative to the insulators, semiconductors have the effect of buffering the difference in dielectric constant between the matrix and the functional particles. Moreover, the interface regulation of the semiconductor can also avoid the leakage conduction current and help the polarization of the substrate. In the semiconductor modification, there are inorganic and organic materials. Among them, as typical organic and inorganic materials, zinc

oxide (ZnO) [28–30] and polydopamine(PDA) [31,32] are widely used in the modification of composites for better optical and electrical properties. This modified composites by ZnO and PDA could be used in electrical storage [33–36], liquid crystal displays, thin-film transistors, light-emitting diodes, photocatalytic, photoelectrochemical and photoelectrochemical devices, etc. [37–40]. However, for the same semiconductor, the difference between the surface modification of inorganic and organic semiconductors for the same material is rarely reported.

Silver rods as a functional filler can increase the response rate of dielectric composites, so that the material can obtain a higher polarization ability at low voltage, thereby improving energy storage density at low voltage. Adding silver alone will increase the conductive loss of composites; therefore, semiconductors are used to modify the surface. In this paper, two pristine core-shell nanorods, Ag@ZnO and Ag@PDA, and their PVDF matrix composites were prepared. The microstructure, dielectric and electrical storage performance of composites were tested. The effects of the ZnO and PDA shells on the polarization mechanism of PVDF were investigated.

Experiments

Material

Silver nitrate (AgNO_3), polyvinylpyrrolidone (PVP), ethylene glycol ($(\text{CH}_2\text{OH})_2$) and *N, N'*-dimethylformamide (DMF) were offered by Nanjing Runsheng Petrochemical Co., Ltd.; zinc acetate dihydrate ($\text{C}_4\text{H}_{10}\text{O}_6\text{Zn}$) and dopamine hydrochloride were purchased from Shanghai Aladdin Biochemical Technology Co., Ltd. Polyvinylidene fluoride (PVDF) ($M_v = 30,000$) were supplied by Guangzhou Xingfeng Chemical Material Co., Ltd.; All chemicals were used without further purification.

Preparation of core-shell nanorods and its composites

The synthesis methods of Ag nanorods can be found in our reported paper [26]. The nucleation of core-shell nanorods is shown in Fig. 1. The preparation process of Ag@PDA: A buffer solution with a pH of 8.5 was prepared by mixing hydrochloric acid and acetic acid, and then the Ag nanorods and dopamine

hydrochloride were placed into the solution with a mass ratio of 1.5:1, wherein the concentration of dopamine in the solution was 1 g/L. The reaction solution was reacted at 50 °C for 4 h under reflux. After the reaction, nanorods were harvested by centrifugation, then washing and drying.

The preparation process of Ag@ZnO: 12 ml of distilled water containing 0.15 g of Ag nanorods and 0.61 g of zinc acetate were ultrasonic-processed for 20 min. Then, the reaction solution was transferred into a 50 ml hydrothermal reaction autoclave; 12 ml of NaOH aqueous solution was added, sealed and put it in a 170 °C oven for 12 h. After the reaction, nanorods were harvested by centrifugation, then washing and drying.

The preparation of Ag@PDA/PVDF and Ag@ZnO/PVDF composites: The composites were prepared by dispersing the nanorods into the PVDF matrix with different weight contents (5 wt%, 10 wt%, 15 wt%, 20 wt%). Firstly, the weighed nanorods were added into 50 ml DMF to ultrasonic dispersion for 1 h; then, 10.25 g PVDF powder was added into the mixed solution and continuously ultrasonic-dispersed for 3 h. After the dispersion, the mixture was cast onto a clean glass plate and subsequently dried in an oven for 4 h at 80 °C. Finally, the obtained thin films were hot-pressed at 180 °C by 10 MPa to prepare the composite films.

Results and discussion

To observe the synthesis of core-shell particles, their micro-morphology was tested. Figure 2 shows the morphology results of Ag nanorods before and after ZnO coating. As shown in Fig. 2a–c, the core-shell nanorods exhibit a uniform and rod-like morphology, the average length of the nanorods is 2 μm and their effective diameter is about 120 nm. All surfaces of core-shell nanorods are very rough, coated by condensed elliptical ZnO particles. The formation of these rough surfaces should be attributed to the supercritical state of a hydrothermal reaction during the formation of the ZnO shell, which provided high temperature and large pressure which promoted the adsorption and growth of crystalline ZnO nanoparticles on the surface of the Ag nanorod. The TEM image in Fig. 2d, e accurately proves the existence of the core-shell structure in which the middle dark part is the nano-Ag core, while the outer relatively

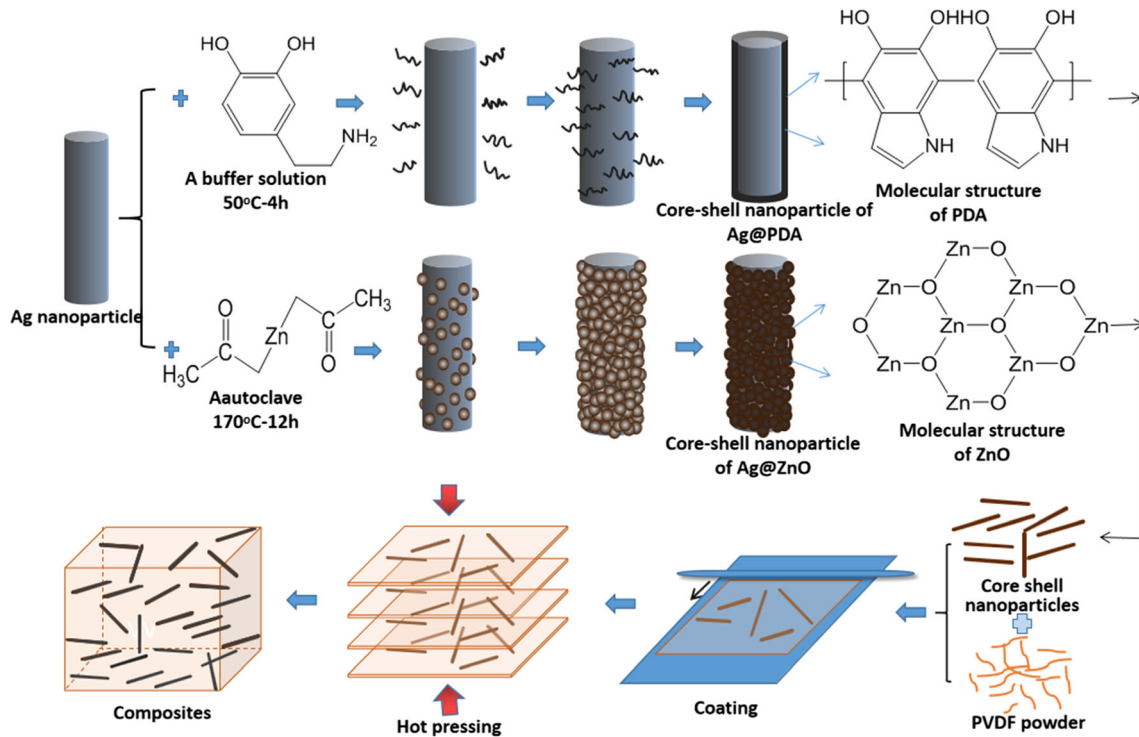


Figure 1 Process illustration of core-shell nanorods synthesis and the preparation of composites.

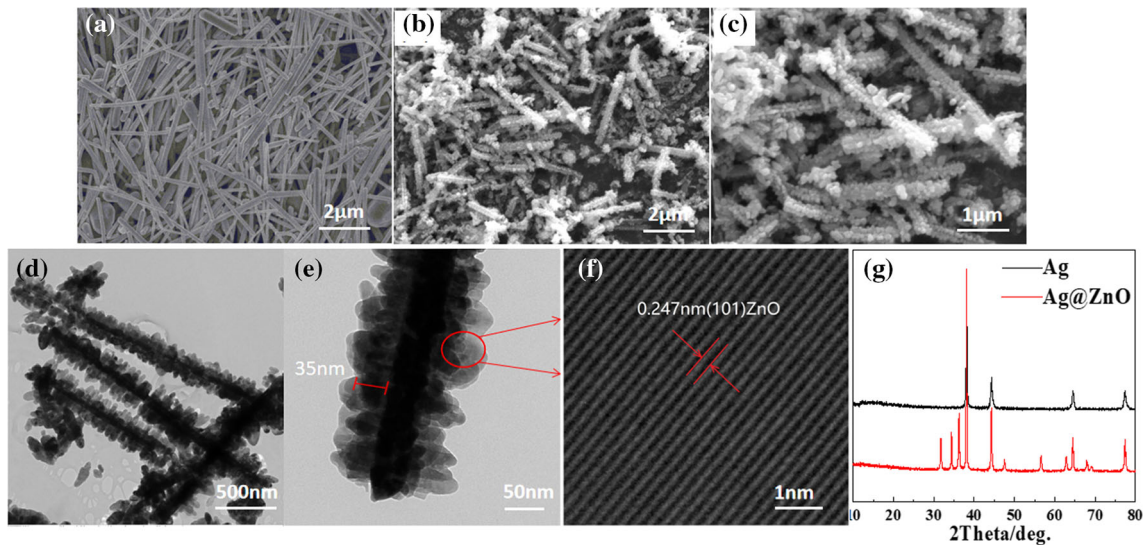


Figure 2 (a) SEM overview of Ag rod; (b, c) SEM overview of the Ag@ZnO nanorods; (d, e) TEM of the Ag@ZnO nanorods; (f) HRTEM of the ZnO shell; (g) Comparison XRD pattern of the nanorods before and after coating.

light part is the ZnO shell. Since the growth of ZnO is formed by the accumulation of microparticles, the effective thickness of the ZnO shell is about 35 nm. Figure 2g shows the XRD spectra of Ag nanorods before and after ZnO coating. As shown in Fig. 2g, the Ag@ZnO nanorods showed a new peak which is the standard diffraction peak of ZnO (see in the

PDF#36–1451 standard card). The occurrence of this diffraction peak also proved the formation of the ZnO shell. Figure 2f shows a partially magnified HRTEM image of the ZnO shell, the distance of the ZnO atom lattice planes is 0.247 nm, which corresponds to the ZnO (101) peak at a relatively strong absorption angle of 36.2°.

Figure 3 shows the morphology results of Ag nanorods before and after PDA coating. As shown in Fig. 3a–c, after coating, the core–shell Ag@PDA nanorods exhibit a smooth and uniform rod-like structure, which is much different from the Ag@ZnO nanorods. The length of the nanorods is about 2 μm and the width is about 120 nm. Compared to the ZnO shell, the polymerization of PDA is a mild reaction, so the resulting shell is smooth and evenly distributed around the Ag particles. The TEM image in Fig. 3d, e also successfully demonstrates the generation of core–shell structures. In general, increasing the molar ratio of the PDA precursor to the Ag nanorods can gradually increase the thickness of the shell. The calculated average thickness of the PDA shell obtained in this experiment is 35 nm, which is almost the same as that of the ZnO shell.

In order to observe the dispersibility of the nanorods in the matrix, we observed the SEM images of the cross section of the composite material. As shown in Fig. 4, with the mass percentage of the two kinds of nanorods increases, the number of particles in the cross section of the composites increases obviously. It is worth noting that within the scope of this experimental design, there was no obvious agglomeration for both Ag@ZnO and Ag@PDA nanorods in the PVDF matrix. Moreover, the nanorods still maintain a rod-like structure, indicating that the core–shell particles are relatively stable, and there

are no obvious voids or cracks in the interfaces between nanorods and the PVDF matrix. Moreover, for composites with a relatively low filler's loading (below 15 wt%), the cross section of the Ag@PDA/PVDF composites is much smoother than the Ag@ZnO/PVDF ones. This can be attributed to the fact that the PDA shell is also a polymer and can be better combined with a polymer matrix with a similar structure. In contrast, the ZnO shell exhibits more occlusal bonding with the PVDF matrix, then resulting in the fracture of Ag@ZnO/PVDF in a brittle fracture mode.

To observe the effect of nanoparticle addition on the crystallization behavior of the PVDF matrix, we performed XRD on the composite. As shown in Fig. 5, after the introduction of the nanorods, there appeared some new peaks and the main phase of the PVDF matrix shifted. For example, for all the composites, there are some common peaks of the Ag crystal at 38.15° , 44.32° , 64.28° and 77.53° which corresponds to the typical crystal planes of Ag at (111), (200), (220) and (311), as proved by PDF#36 1451. Moreover, for the Ag@ZnO/PVDF composites, there also appeared some new peaks at 31.78° , 34.48° , 36.20° corresponding to the crystal plane of ZnO at (100) (002) (101) in PDF#36–1451 card. However, for the Ag@PDA/PVDF composite, there is no new diffraction peak appearing in the XRD diffractogram as its amorphous. Besides, the characteristic peaks

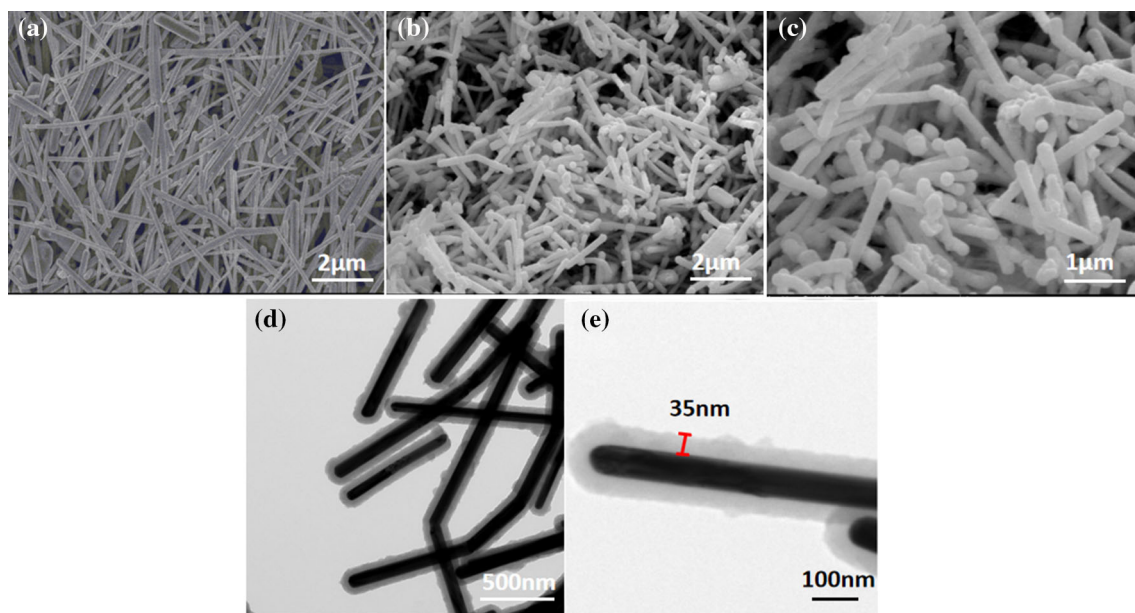


Figure 3 (a) SEM overview of Ag rod; (b, c) SEM overview of the Ag@PDA nanorods; (d, e) TEM of the Ag@PDA nanorods.

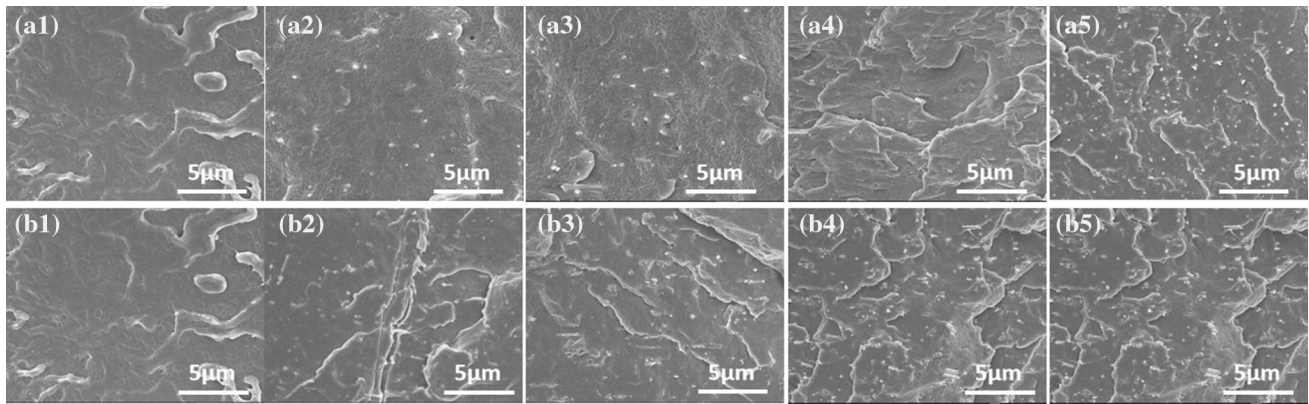
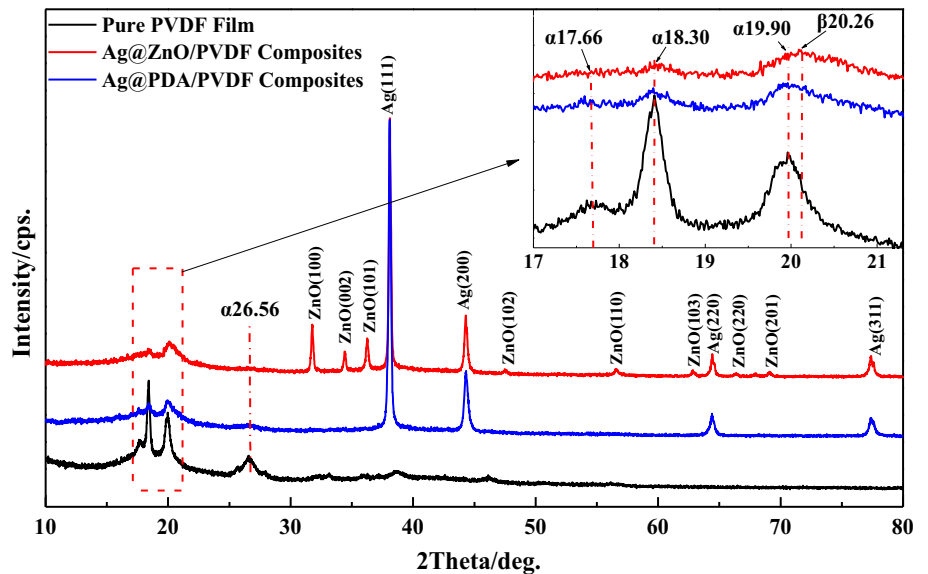


Figure 4 Cross-sectional SEM of (a) Ag@PDA/PVDF and (b) Ag@ZnO/PVDF composites with different addition amounts (0 wt%, 5 wt%, 10 wt%, 15 wt%, 20 wt%).

Figure 5 XRD diffractogram of Ag@PDA/PVDF and Ag@ZnO/PVDF composites with 10 wt% addition.



intensity of the PVDF matrix changed greatly. For example, in both of composites, the absorption peaks also appear at 17.6°, 18.3°, 19.9° and 26.5° which corresponds to the $\alpha(100)$, $\alpha(020)$, $\alpha(110)$ and $\alpha(021)$ phases of PVDF crystals, respectively [41], but the intensity is significantly weakened compared to the pure one. Also the peak intensity of composite material around 20.0° is slightly higher and wider than that of 18.0°, which is opposite to the trend of the pure film. This is credited with that the peak of $\beta(110)(200)$ at 20.26° and the peak of $\gamma(110)$ at 20.04° of PVDF matrix in composite also appeared near 20.0°, not only the peak of $\alpha(110)$ at 19.9°.

To better observe this phase transition, we conducted FTIR experiments on the composite material. As Fig. 6 shows, there is also a huge change around the 840 cm^{-1} absorption range; all the composites

represent a stronger absorption than the pure one. The Ag@ZnO/PVDF composites present a broad mixture of β and γ absorption at 840 cm^{-1} and a new γ absorption peak at 812 cm^{-1} [41]. These changes in peaks suggest that the polarity of PVDF has changed, which would take a large effect on the dielectric properties of the composites. Usually, these changes of β and γ phase of PVDF molecules would improve the dielectric constant of the composite than before.

To better characterize the dielectric properties of the composite materials, we tested the dielectric properties as a function of frequency. As shown in Figs. 7a-1, b-1 and 8d, for these two types of particles, the dielectric constant of both Ag@PDA/PVDF and Ag@ZnO/PVDF composites increased with the addition of nanorods, they showed almost the same ability to modify the dielectric constant of the matrix,

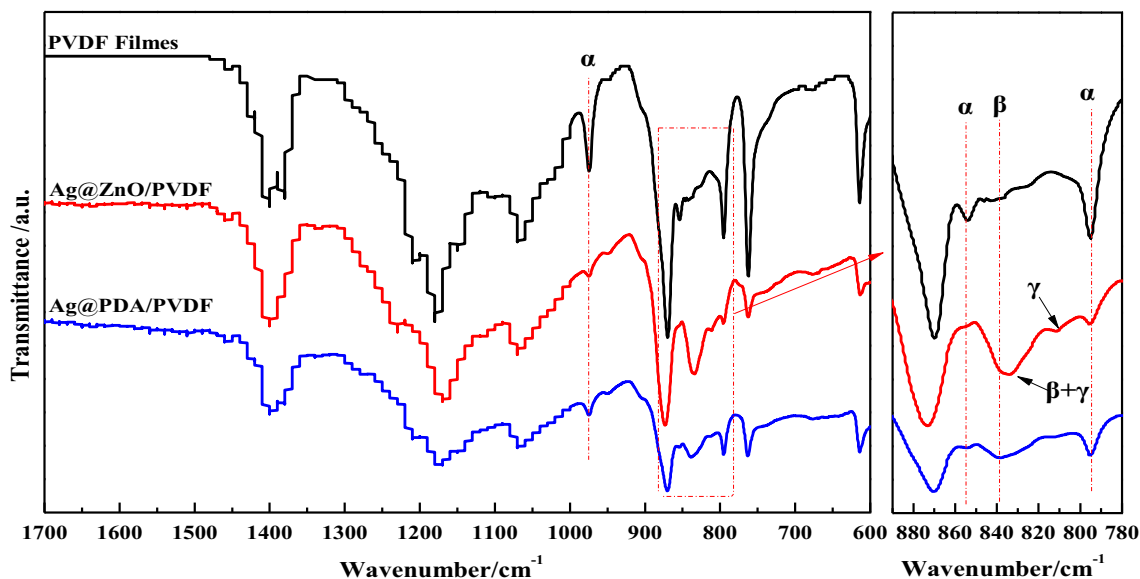


Figure 6 FTIR spectrogram of Ag@PDA/PVDF and Ag@ZnO/PVDF composites with 10 wt% addition.

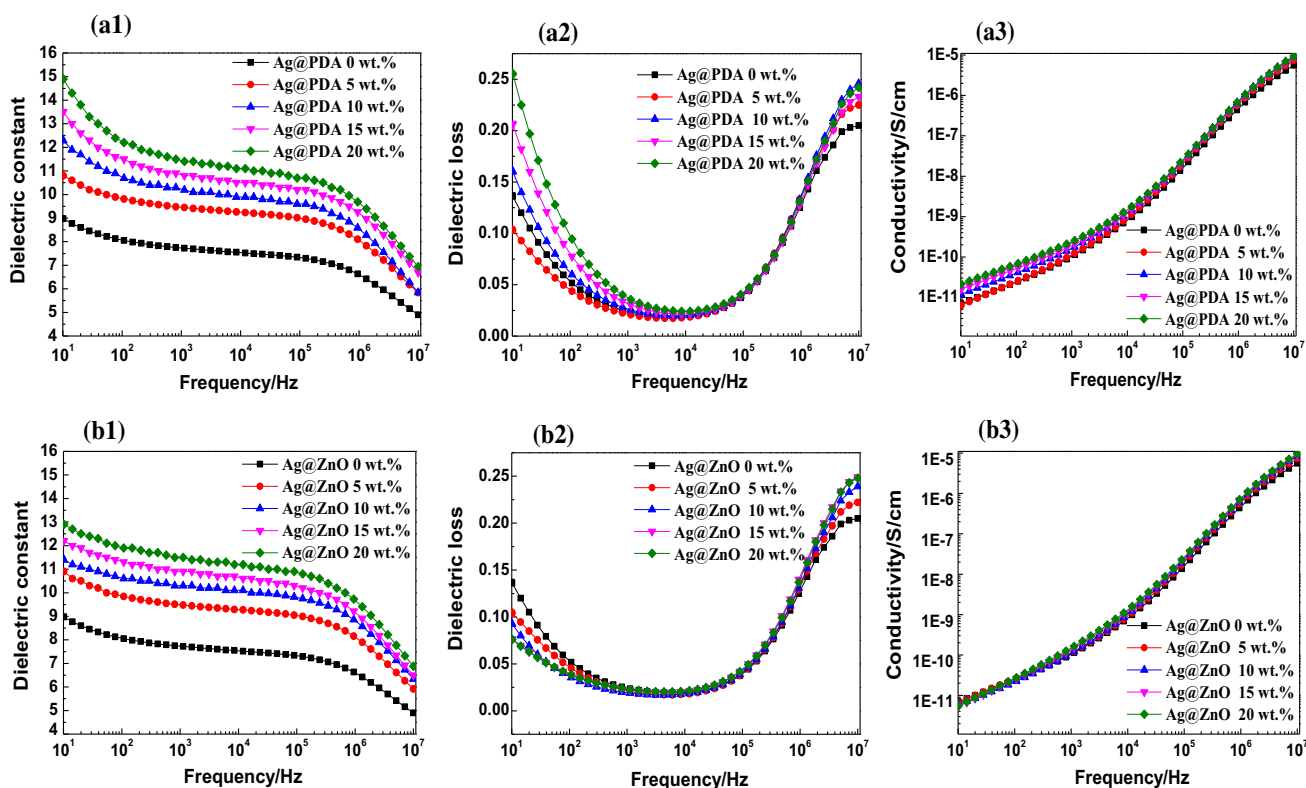
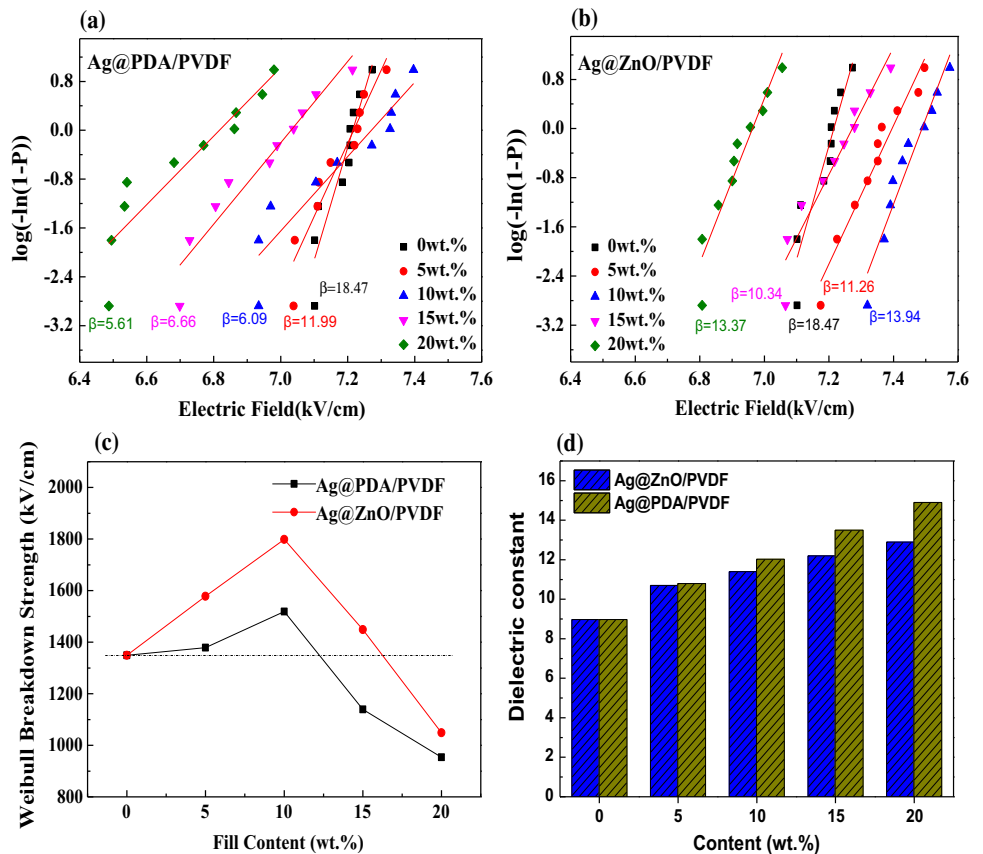


Figure 7 Dielectric constant, dielectric loss and conductivity of (a) Ag@PDA/PVDF and (b) Ag@ZnO/PVDF as a function of testing frequency.

and the dielectric constant of the PDA modification component is slightly higher than that of ZnO. For the entire dielectric material, the magnitude of the vector dipole moment is proportional to the charge.

So the major improvement is attributed to a better in-store charge ability of Ag nanorods under the action of an alternating electric field than for the polymer, at the same time, 1D nanoparticles have a larger electric

Figure 8 Weibull breakdown field of (a) Ag@PDA/PVDF composites, (b) Ag@ZnO/PVDF composites and (c) Weibull breakdown strength of composites, (d) dielectric constant of Ag@PDA/PVDF and Ag@ZnO/PVDF composites with different contents at 10 Hz.



dipole moment than 0D nanoparticles, which could amplify the electron displacement polarization in the matrix. The difference in the degree of polarization caused by PDA and ZnO is mainly due to the difference in polarization behavior. PDA is a polar dielectric, under the action of an electric field, electronic polarization and steering polarization will occur. However, ZnO belongs to the ionic dielectrics, which mainly generates electronic polarization and ionic polarization. Usually, to establish steering polarization spend more time than electronic polarization and ionic polarization behaviors. Moreover, the PDA itself has an electric dipole moment, so the polarization degree of PDA is higher than for ZnO in the low-frequency range, when the frequency increases, this polarization gap is weakened.

Furthermore, as shown in Fig. 7a-2, b-2, after the modification by adding core-shell nanorods, the overall dielectric loss of the composites remains at a low level. For the dielectric loss of Ag@PDA component, only at 5 wt% filler amount it is lower than that of the pure film at low frequency. The others composites dielectric loss increases with different

fillers in different frequency ranges, but the overall loss is still lower than 0.25. On the other hand, below a frequency of 10^3 Hz, the loss of composites of Ag@ZnO is all lower than the pure film, then the dielectric loss slowly increases as the frequency increases. At low frequencies, the difference in dielectric loss between the Ag@PDA and Ag@ZnO composites is closely related to the polarization behavior. Due to the inherent electric dipole moment of the PDA, it undergoes steering polarization under an electric field. This behavior takes a longer time than the ZnO ion polarization, and the energy cannot be fully recovered. The addition of an Ag core will amplify this effect, so the dielectric loss will be greater. At high frequencies, the dielectric loss is mainly due to the relaxation loss of the polar base. The introduction of these two core-shell particles in PVDF is equivalent to the introduction of impurities in the matrix crystal, so the loss of both composite materials is higher than that of the pure film [42].

Figure 7a-3, b-3 shows the spectrum of the conductivity of the composites as a function of frequency. As the amount of nanorods added increases,

the conductivity of the two composites shows different changes. The Ag@PDA/PVDF composites showed an overall upward trend in electrical conductivity, while the Ag@ZnO/PVDF composites did not change significantly. Electrical conductivity is an important parameter for evaluating the mobility of carriers in dielectrics. The experimental results indicate that ZnO has a stronger ability to restrict carrier migration than PDA. This may be closely related to the ZnO crystal structure, as the high crystallinity has a higher band gap than the disordered state. Therefore, Ag@ZnO/PVDF has a stronger ability to bind carriers.

The electrical breakdown strength of composite materials is an important parameter in the calculation of energy storage density, and it usually described by the Weibull cumulative distribution function with two parameters (Eqs. 1–3), as in Eq. (1).

$$P(E) = 1 - \exp\left[-\left(\frac{E}{E_0}\right)^\beta\right]. \quad (1)$$

In Eq. (1), $P(E)$ is the cumulative failure probability; E is the breakdown field strength; β is the shape parameter; E_0 is the breakdown field strength at $P(E) = 63.28\%$. Taking the logarithm of both sides of Eq. (1), one obtains Eq. (2):

$$\ln[-\ln(1 - p)] = \beta(\ln E - \ln E_0). \quad (2)$$

For each corresponding field strength E_0 , a P value can be calculated, which is calculated by Eq. (3), where i indicates that the E values are arranged from small to large; n indicating the number of tests of each sample.

$$p = \frac{i - 0.5}{n + 0.25}. \quad (3)$$

The correspondence between $\ln(-\ln(1 - P(E)))$ and $\ln E$ is shown in Fig. 8a–c. As shown, with the addition of both Ag@PDA and Ag@ZnO core-shell nanorods, the overall breakdown strength of the composites shows a trend of rising first and then decreasing. The Ag@ZnO/PVDF composites show better resistance to breakdown than the Ag@PDA/PVDF composites. Among them, when the addition amount is 10 wt%, the breakdown strength of Ag@ZnO/PVDF composites is ~ 1799 kV/cm ($\beta = 13.94$), and Ag@PDA/PVDF is 1519 kV/cm ($\beta = 6.09$), which is 33.35% and 12.6% higher than that of a pure film 1349 kV/cm, respectively. Usually,

the breakdown field strength of a material is closely related to its ability to limit the space charge to form a leakage current [43]. In addition, for the leakage current test of materials as shown in Fig. 9d, the leakage currents of ZnO and PDA at 200 kV/cm are $3.37E^{-8}$ A/cm² and $4.153.37E^{-8}$ A/cm², respectively. It shows that under the same conditions, ZnO has a stronger ability to limit space charge than PDA, which is in agreement with the results of the Weibull analysis.

To better demonstrate the polarization behavior of different composites along with the electric field strength, and to calculate the energy storage density and cycle efficiency of the material, the change curves of electric displacement and electrical field strength of two kinds of core-shell (Ag@PDA, Ag@ZnO) nanorods under different additions are tested and the results are shown in Fig. 9a,b. As shown, the 10 wt% Ag@PDA/PVDF composites at 1500 kV/cm obtained the maximum polarization value of $5.60 \mu\text{C}/\text{cm}^2$, while the 10 wt% Ag@ZnO/PVDF composites reached the maximum polarization value of $6.84 \mu\text{C}/\text{cm}^2$ in 1800 kV/cm. It is assumed that the maximum polarization degree of the material is related to the breakdown field strength. However, under the same field strength and fillers' amount, as shown in Fig. 9c, the PDA shows better polarization performance, which is consistent with the dielectric constant results.

The difference in the polarization strength of the two types of semiconductor core-shell particles is largely due to the different aggregate states of the shell materials. The simplified mechanism is shown in Fig. 10. As a typical amorphous polymer, the PDA layer between Ag nanorods and the PVDF matrix also acts as an amorphous phase with a good fusion. It is easy to pass polarization when an electric field is applied. However, ZnO has a highly regular crystal structure [44], and when it acts as an interfacial layer, it will have a barrier effect during the polarization process of polymeric molecules, which could weaken the polarization of composites and reduce the accumulation of space charge to a certain extent. At the same time, amorphous polymers will also generate more voids during the behavior of turning polarization, causing higher dielectric loss, which will further affect the charge/discharge efficiency of the composites.

The polarization and depolarization behavior of a dielectric under an external electric field represents

Figure 9 D–E curve of (a) Ag@PDA/PVDF composites with different additions; (b) Ag@ZnO/PVDF composites with different additions; (c) Ag@PDA/PVDF and Ag@ZnO/PVDF with 10 wt% addition at 1000 kV/cm; (d) leakage current density for Ag@PDA/PVDF and Ag@ZnO/PVDF composites with 10 wt% addition.

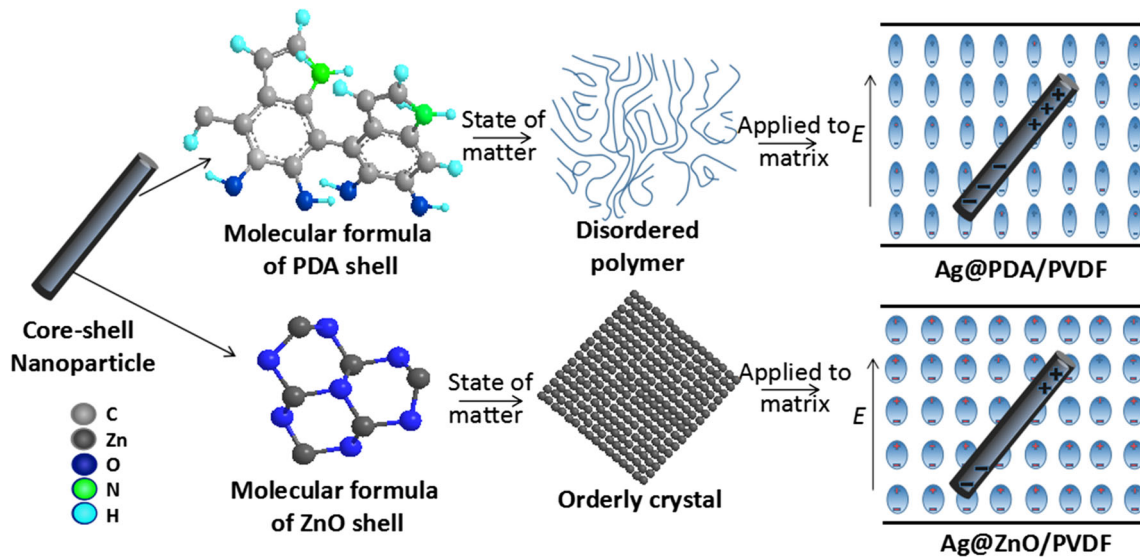
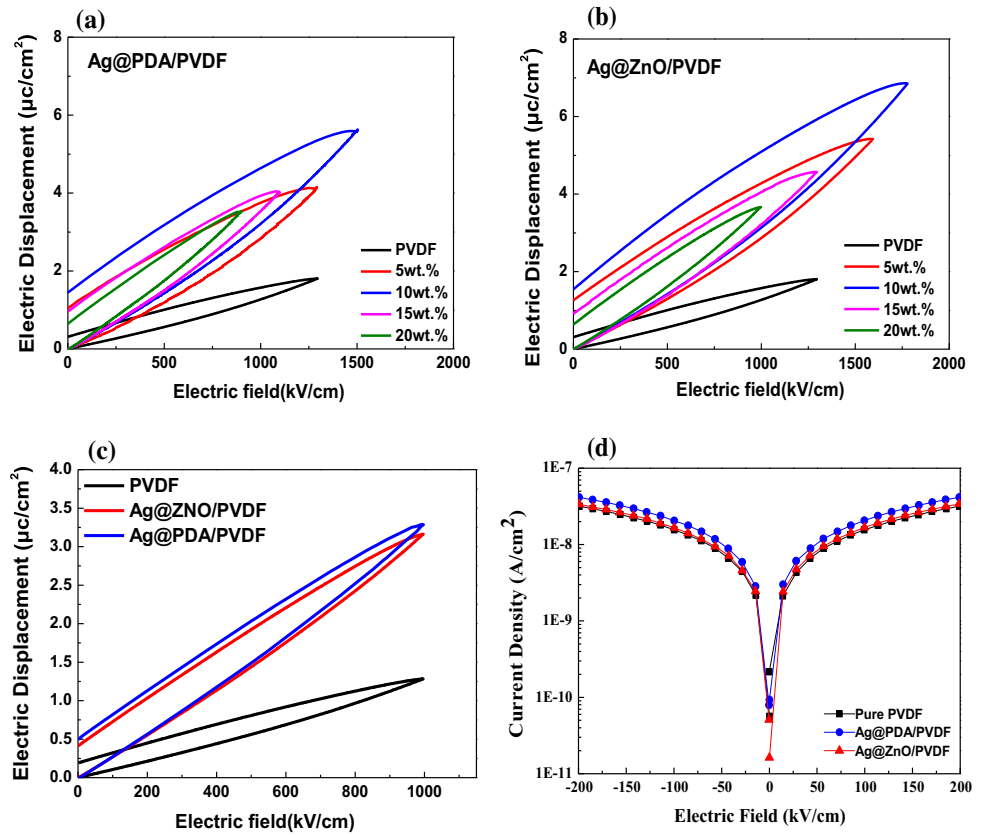


Figure 10 Illustration of polarization process for composites.

the charging and discharging process of a dielectric capacitor, respectively. In principle, the energy storage density of a nonlinear dielectric can be calculated from the applied electric field and electric displacement using Eq. (4).

$$U = \int E dD \tag{4}$$

where E is the electric field strength and D is the electrical displacement. The charge and discharge efficiency of the dielectric material can be calculated by Eq. (5).

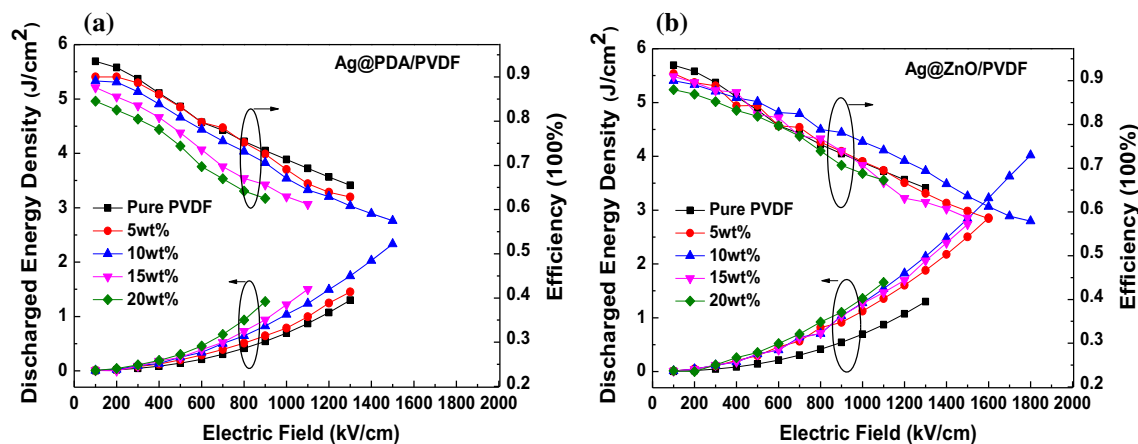


Figure 11 Energy storage density and charge/discharge efficiency of (a) Ag@PDA/PVDF and (b) Ag@ZnO/PVDF composites with different additions.

Table 1 Energy storage densities compared with other PVDF-based composites

Samples	U_e max (J/cm^3)	η	References
1 wt%rGO-Ag/PVDF	0.26	–	[45]
5 wt% GP- Al_2O_3 /PVDF-HFP	1.21	0.58	[46]
10 wt%PPFPA@BST-P(VDF-HFP)	2.25	0.62	[47]
10 vol% TiO_2 @dopa/PVDF	1.25	0.42	[48]
10 vol% TiO_2 -BT@dopa/PVDF	2.60	0.59	[48]
0.075 wt%Ag@Thiol-PVDF	3.19	–	[49]
0.05 wt%Ag@Thiol-PVDF	3.87	–	[49]
10 wt%Ag@PDA/PVDF	2.33	0.57	This work
10 wt%Ag@ZnO/PVDF	4.02	0.58	This work

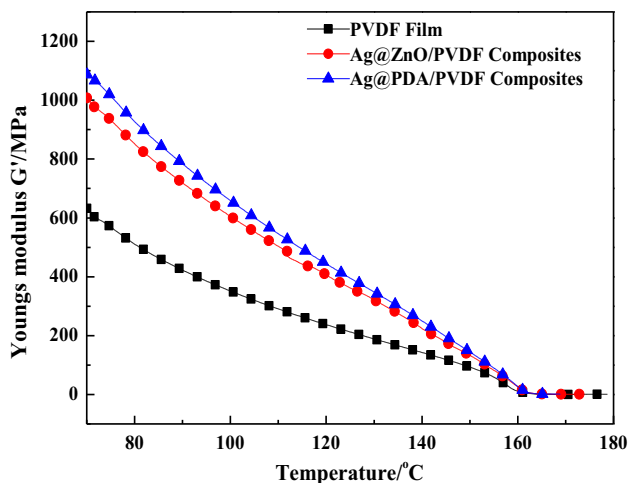


Figure 12 Dynamic mechanical analysis of PVDF film, Ag@ZnO/PVDF and Ag@PDA /PVDF composites with 10wt% adding content.

$$\eta = \frac{U_{dis}}{U_{dis} + U_{loss}} \quad (5)$$

where U_{dis} is the discharge energy and U_{loss} is the loss energy which corresponds to the area integral value in the D - E curve in Fig. 9.

Via calculation, we obtain the relationship spectrum between the material's energy storage density, charge/discharge efficiency and breakdown strength in Fig. 11. In the case of 10 wt% fillers' content and before breakdown strength, the energy storage densities of Ag@PDA/PVDF and Ag@ZnO/PVDF composites are 2.34 J/cm^3 and 4.02 J/cm^3 , which is an increase of 79.53% and 209.2% compared to pure PVDF films, respectively. The energy storage densities compared with other PVDF-based composites are shown in Table 1. It is worth noting that while Ag@ZnO/PVDF increases the energy storage density, it still maintains a good charge and discharge efficiency. However, due to the good compatibility of the PDA and the matrix, the Ag@PDA/PVDF composites perform better in terms of dynamic mechanical behavior. As shown in Fig. 12 at the initial temperature of 50 °C, the Young's modulus of the Ag@ZnO/

PVDF and Ag@PDA/PVDF is 1019.83 MPa and 1103.39 MPa, compared with the one of a pure PVDF film 633.18 MPa, it is increased by 61.06% and 74.26%, respectively.

Conclusion

We successfully synthesized two kinds of 1D core-shell nanorods (Ag@PDA, Ag@ZnO) and their PVDF matrix composites. The different effects on the dielectric properties between inorganic ZnO and organic PDA shells have been investigated. Microstructural analysis showed that the Ag@PDA and Ag@ZnO nanorods could be evenly dispersed in a PVDF matrix without obvious aggregation. In the case of 10 wt% fillers' content and before breakdown strength, the energy storage densities of Ag@PDA/PVDF and Ag@ZnO/PVDF composites are 79.53% and 209.2% higher than that of pure PVDF films, respectively. Moreover, the charge/discharge efficiency of Ag@ZnO/PVDF composite is also higher than that of pure PVDF and Ag@PDA/PVDF composite. It is worth to note that at 1800 kV/cm testing electrical strength, the discharge energy storage density of the Ag@ZnO/PVDF composites reaches to 4.02 J/cm³. In summary, this PVDF-based composite doped with Ag nanorods decorated by inorganic ZnO shell exhibits a higher ability to constrain electrons than PDA, which is beneficial to the performance regarding dielectric properties.

Acknowledgements

This work was supported by the National Natural Science Foundation of China (Nos. 51677045, 51603057) and the Harbin Science and Technology Innovation Talents Project (No. 2016RAQXJ059).

References

- [1] Baer E, Zhu L (2017) 50th anniversary perspective: dielectric phenomena in polymers and multilayered dielectric films. *Macromolecules* 50:2239–2256. <https://doi.org/10.1021/acs.macromol.6b02669>
- [2] Gong HH, Miao B, Zhang X, Lu JY, Zhang ZC (2016) High-field antiferroelectric-like behavior in uniaxially stretched poly (vinylidene fluoride-trifluoroethylene-chlorotrifluoroethylene)-grafted-poly (methyl methacrylate) films with high energy density. *RSC Adv* 6:1589–1599. <https://doi.org/10.1039/c5ra22617a>
- [3] Opris DM (2018) Polar elastomers as novel materials for electromechanical actuator applications. *Adv Mater* 30:1703678. <https://doi.org/10.1002/adma.201703678>
- [4] Palneedi H, Peddigari M, Hwang GT, Jeong DY, Ryu J (2018) High-performance dielectric ceramic films for energy storage capacitors: progress and outlook. *Adv Funct Mater* 28:1803665. <https://doi.org/10.1002/adfm.201803665>
- [5] Wen RM, Guo JM, Zhao CL, Liu YQ (2018) Nanocomposite capacitors with significantly enhanced energy density and breakdown strength utilizing a small loading of monolayer titania. *Adv Mater Interfaces* 5:1701088. <https://doi.org/10.1002/admi.201701088>
- [6] Yang LT, Kong X, Li F et al (2019) Perovskite lead-free dielectrics for energy storage applications. *Progr Mater Sci* 102:72–108. <https://doi.org/10.1016/j.pmatsci.2018.12.005>
- [7] Wei HG, Wang H, Xia YJ et al (2018) An overview of lead-free piezoelectric materials and devices. *J Mater Chem C* 6:12446–12467. <https://doi.org/10.1039/c8tc04515a>
- [8] Surmenev RA, Orlova T, Chernozem RV et al (2019) Hybrid lead-free polymer-based nanocomposites with improved piezoelectric response for biomedical energy-harvesting applications: a review. *Nano Energy* 62:475–506. <https://doi.org/10.1016/j.nanoen.2019.04.090>
- [9] Shi FM, Ma YX, Ma J, Wang PP, Sun WX (2012) Preparation and characterization of PVDF/TiO₂ hybrid membranes with different dosage of nano-TiO₂. *J Membr Sci* 389:522–531. <https://doi.org/10.1016/j.memsci.2011.11.022>
- [10] Zhou MX, Liang RH, Zhou ZY, Dong XL (2018) Novel BaTiO₃-based lead-free ceramic capacitors featuring high energy storage density, high power density, and excellent stability. *J Mater Chem C* 6:8528–8537. <https://doi.org/10.1039/c8tc03003k>
- [11] Shin EY, Cho HJ, Jung S, Yang C, Noh YY (2018) A high-k fluorinated P (VDF-TrFE)-g-PMMA gate dielectric for high-performance flexible field-effect transistors. *Adv Funct Mater* 28:1704780. <https://doi.org/10.1002/adfm.201704780>
- [12] Zhu H, Liu Z, Wang FH (2017) Improved dielectric properties and energy storage density of poly (vinylidene fluoride-co-trifluoroethylene-co-chlorotrifluoroethylene) composite films with aromatic polythiourea. *J Mater Sci* 52:5048–5059. <https://doi.org/10.1007/s10853-016-0742-6>
- [13] Zhang J, Liu D, Han Q et al (2019) Mechanically stretchable piezoelectric poly(vinylidene fluoride)/Boron nitride nanosheets (BNNs) polymer nanocomposites. *Compos Part B Eng* 175:107157. <https://doi.org/10.1016/j.compositesb.2019.107157>
- [14] Wang MJ, Jiao ZY, Chen YP et al (2018) Enhanced thermal conductivity of poly (vinylidene fluoride)/boron nitride

- nanosheet composites at low filler content. *Compos Pt A-Appl Sci Manuf* 109:321–329. <https://doi.org/10.1016/j.compositesa.2018.03.023>
- [15] Bhattacharya G, Fishlock SJ, Pritam A, Roy SS, McLaughlin JA (2020) Recycled red mud-decorated porous 3D graphene for high-energy flexible micro-supercapacitor. *Adv Sustain Syst* 4:1900133. <https://doi.org/10.1002/adsu.201900133>
- [16] Kirubasankar B, Murugadoss V, Lin J et al (2018) In situ grown nickel selenide on graphene nanohybrid electrodes for high energy density asymmetric supercapacitors. *Nanoscale* 10:20414–20425. <https://doi.org/10.1039/c8nr06345a>
- [17] Chen H, Ling M, Hencz L et al (2018) Exploring chemical, mechanical, and electrical functionalities of binders for advanced energy-storage devices. *Chem Rev* 118:8936–8982. <https://doi.org/10.1021/acs.chemrev.8b00241>
- [18] Shen ZH, Wang JJ, Lin YH, Nan CW, Chen LQ, Shen Y (2018) High-throughput phase-field design of high-energy-density polymer nanocomposites. *Adv Mater* 30:1704380. <https://doi.org/10.1002/adma.201704380>
- [19] Prateek VKT, Gupta RK (2016) Recent progress on ferroelectric polymer-based nanocomposites for high energy density capacitors: synthesis, dielectric properties, and future aspects. *Chem Rev* 116:4260–4317. <https://doi.org/10.1021/acs.chemrev.5b00495>
- [20] Pan ZB, Yao LM, Zhai JW, Fu DZ, Shen B, Wang HT (2017) High-energy-density polymer nanocomposites composed of newly structured one-dimensional BaTiO₃@Al₂O₃ nanofibers. *ACS Appl Mater Interfaces* 9:4024–4033. <https://doi.org/10.1021/acsami.6b13663>
- [21] Zhang Y, Zhang CH, Feng Y et al (2019) Excellent energy storage performance and thermal property of polymer-based composite induced by multifunctional one-dimensional nanofibers oriented in-plane direction. *Nano Energy* 56:138–150. <https://doi.org/10.1016/j.nanoen.2018.11.044>
- [22] Feenstra J, Sodano HA (2008) Enhanced active piezoelectric 0–3 nanocomposites fabricated through electrospun nanowires. *J Appl Phys* 103:124108. <https://doi.org/10.1063/1.2939271>
- [23] Wang G, Li JL, Zhang X et al (2019) Ultrahigh energy storage density lead-free multilayers by controlled electrical homogeneity. *Energy Environ Sci* 12:582–588. <https://doi.org/10.1039/c8ee03287d>
- [24] Pan ZB, Yao LM, Zhai JW et al (2016) Excellent energy density of polymer nanocomposites containing BaTiO₃@Al₂O₃ nanofibers induced by moderate interfacial area. *J Mater Chem A* 4:13259–13264. <https://doi.org/10.1039/c6ta05233a>
- [25] Huang XY, Jiang PK (2015) Core-shell structured high-k polymer nanocomposites for energy storage and dielectric applications. *Adv Mater* 27:546–554. <https://doi.org/10.1002/adma.201401310>
- [26] Guan LZ, Liu LZ, Weng L, Zhang XR, Cui WW (2018) Enhancement in energy storage density of polyvinylidene fluoride composites by introduced rod-like core-shell Ag@Al₂O₃ nanorods. *Polymer* 148:39–48. <https://doi.org/10.1016/j.polymer.2018.06.010>
- [27] He DL, Wang Y, Song SL, Liu S, Luo Y, Deng Y (2017) Polymer-based nanocomposites employing Bi₂S₃@SiO₂ nanorods for high dielectric performance: understanding the role of interfacial polarization in semiconductor-insulator core-shell nanostructure. *Compos Sci Technol* 151:25–33. <https://doi.org/10.1016/j.compscitech.2017.08.006>
- [28] Wang S, Zhu BC, Liu MJ, Zhang LY, Yu JG, Zhou MH (2019) Direct Z-scheme ZnO/CdS hierarchical photocatalyst for enhanced photocatalytic H₂-production activity. *Appl Catal B-Environ* 243:19–26. <https://doi.org/10.1016/j.apcatb.2018.10.019>
- [29] Ouyang WX, Teng F, He JH, Fang XS (2019) Enhancing the photoelectric performance of photodetectors based on metal oxide semiconductors by charge-carrier engineering. *Adv Funct Mater* 29:1807672. <https://doi.org/10.1002/adfm.201807672>
- [30] Wu GL, Jia ZR, Cheng YH, Zhang HX, Zhou XF, Wu HJ (2019) Easy synthesis of multi-shelled ZnO hollow spheres and their conversion into hedgehog-like ZnO hollow spheres with superior rate performance for lithium ion batteries. *Appl Surf Sci* 464:472–478. <https://doi.org/10.1016/j.apsusc.2018.09.115>
- [31] Gu HB, Xu XJ, Dong MY et al (2019) Carbon nanospheres induced high negative permittivity in nanosilver-polydopamine metacomposites. *Carbon* 147:550–558. <https://doi.org/10.1016/j.carbon.2019.03.028>
- [32] Lai YX, Zhang CX, Deng Y et al (2019) A novel α -feto-protein-MIP immunosensor based on AuNPs/PTH modified glass carbon electrode. *Chin Chem Lett* 30:160–162. <https://doi.org/10.1016/j.ccllet.2018.07.011>
- [33] Li Y, Zhang L, Yu LJ et al (2020) Study of the structure, electrical properties, and energy storage performance of ZnO-modified Ba_{0.65}Sr_{0.245}Bi_{0.07}TiO₃ Pb-free ceramics. *Ceram Int* 46:8–16. <https://doi.org/10.1016/j.ceramint.2019.08.111>
- [34] Zhang L, Pu YP, Chen M, Wei TC, Peng X (2020) Novel Na_{0.5}Bi_{0.5}TiO₃ based, lead-free energy storage ceramics with high power and energy density and excellent high-temperature stability. *Chem Eng J* 383:123154. <https://doi.org/10.1016/j.cej.2019.123154>
- [35] Zhang L, Song F, Lin X, Wang D (2020) High-dielectric-permittivity silicone rubbers incorporated with polydopamine-modified ceramics and their potential application

- as dielectric elastomer generator. *Mater Chem Phys* 241:122373. <https://doi.org/10.1016/j.matchemphys.2019.122373>
- [36] Yang Z, Wang J, Hu YL, Deng CY, Zhu KJ, Qiu JH (2020) Simultaneously improved dielectric constant and breakdown strength of PVDF/Nd-BaTiO₃ fiber composite films via the surface modification and subtle filler content modulation. *Compos Pt A-Appl Sci Manuf* 128:105675. <https://doi.org/10.1016/j.compositesa.2019.105675>
- [37] Liang F-X, Gao Y, Xie C, Tong X-W, Li Z-J, Luo L-B (2018) Recent advances in the fabrication of graphene–ZnO heterojunctions for optoelectronic device applications. *J Mater Chem C* 6:3815–3833. <https://doi.org/10.1039/c8tc00172c>
- [38] Ding M, Guo Z, Zhou L et al (2018) One-dimensional zinc oxide nanomaterials for application in high-performance advanced optoelectronic devices. *Crystals* 8:223. <https://doi.org/10.3390/cryst8050223>
- [39] Duan L, Wang L, Li F, Li F, Sun L (2015) Highly efficient bioinspired molecular Ru water oxidation catalysts with negatively charged backbone ligands. *Account Chem Res* 48:2084–2096. <https://doi.org/10.1021/acs.accounts.5b00149>
- [40] Yu Y, Huang Z, Zhou Y et al (2019) Facile and highly sensitive photoelectrochemical biosensing platform based on hierarchical architected polydopamine/tungsten oxide nanocomposite film. *Biosens Bioelectr* 126:1–6. <https://doi.org/10.1016/j.bios.2018.10.026>
- [41] Gebrekrstos A, Madras G, Bose S (2019) Journey of electroactive β -polymorph of poly (vinylidene fluoride) from crystal growth to design to applications. *Cryst Growth Des* 19:5441–5456. <https://doi.org/10.1021/acs.cgd.9b00381>
- [42] Agrawal A, Cho SH, Zandi O, Ghosh S, Johns RW, Milliron DJ (2018) Localized surface plasmon resonance in semiconductor nanocrystals. *Chem Rev* 118:3121–3207. <https://doi.org/10.1021/acs.chemrev.7b00613>
- [43] Ding F, Pors A, Bozhevolnyi SI (2018) Gradient metasurfaces: a review of fundamentals and applications. *Rep Progr Phys* 81:026401. <https://doi.org/10.1088/1361-6633/aa8732>
- [44] Li AB, Singh S, Sievenpiper D (2018) Metasurfaces and their applications. *Nanophotonics* 7:989–1011. <https://doi.org/10.1515/nanoph-2017-0120>
- [45] Pusty M, Sinha L, Shirage P (2018) A flexible self-poled piezoelectric nanogenerator based on a rGO–Ag/PVDF nanocomposite. *N J Chem* 43:284–294. <https://doi.org/10.1039/C8NJ04751K>
- [46] Li J, Yin J, Yang C et al (2019) Enhanced dielectric performance and energy storage of PVDF-HFP-based composites induced by surface charged Al₂O₃. *J Polym Sci Part B Polym Phys* 57:574–583. <https://doi.org/10.1002/polb.24814>
- [47] Wang S, Huang X, Wang G, Wang Y, Jinliang H, Jiang P (2015) Increasing the energy efficiency and breakdown strength of high-energy-density polymer nanocomposites by engineering the Ba_{0.7}Sr_{0.3}TiO₃ nanowire surface via reversible addition–fragmentation chain transfer polymerization. *J Phys Chem C* 119:25307. <https://doi.org/10.1021/acs.jpcc.5b09066>
- [48] Prateek RB, Siddiqui S, Garg A, Gupta RK (2019) Significantly enhanced energy density by tailoring the interface in hierarchically structured TiO₂–BaTiO₃–TiO₂ nanofillers in PVDF-based thin-film polymer nanocomposites. *ACS Appl Mater Interfaces* 11:14329–14339. <https://doi.org/10.1021/acsaami.9b01359>
- [49] Sarkarat M, Meddeb A, Komarneni S, Ounaies Z (2019) Impact of stabilizer on in situ formation of Ag nanoparticles in polyvinylidene fluoride (PVDF) matrix. *MRS Adv* 4:2103–2108. <https://doi.org/10.1557/adv.2019.236>

Publisher's Note Springer Nature remains neutral with regard to jurisdictional claims in published maps and institutional affiliations.